Time-domain analysis of quantum states of light: noise characterization and homodyne tomography

Alessandro Zavatta

Istituto Nazionale di Ottica Applicata, Largo E. Fermi, 6, 50125, Florence, Italy, and Department of Systems and Computer Science, University of Firenze, Florence, Italy

Marco Bellini and Pier Luigi Ramazza

Istituto Nazionale di Ottica Applicata, Largo E. Fermi, 6, 50125, Florence, Italy, and Istituto Nazionale di Fisica per la Materia, Unità di Firenze, Florence, Italy

Francesco Marin and Fortunato Tito Arecchi

Istituto Nazionale di Ottica Applicata, Largo E. Fermi, 6, 50125, Florence, Italy, and Department of Physics, University of Firenze, Florence, Italy

Received July 11, 2001

We measured the time-domain quantum statistics of a pulsed, high-repetition-rate optical field by balanced homodyne detection. The measuring apparatus discriminates the time scales on which intrinsic quantum fluctuations prevail from those scales for which technical noise is overwhelming. A tomographic reconstruction of weak coherent states with various average photon numbers demonstrates the potential ability of the system to measure high-repetition-rate, time-resolved signals. Possible extensions to other physical situations are discussed.

OCIS codes: 270.5570, 030.5290.

1. INTRODUCTION

Homodyne detection has been extensively used in quantum optics[1,2] to produce tomographic reconstructions of cw fields, such as vacuum, coherent, and squeezed states.[3] To gain access to quantum states that exhibit stronger nonclassical features, one has to exploit the higher nonlinearities made available by the high peak intensities of pulsed lasers. A frequency-domain approach, with a spectral analysis of the difference current in the homodyne photodetectors, was originally developed for studying the noise in the field quadratures at definite detection frequencies.[4]

Subsequently, pulsed balanced homodyne detection, consisting of the measurement of integrated photocurrents on single pulses, was adopted to produce a full reconstruction of weak field states.[5,6] The task of performing this time-domain homodyne detection is, however, quite demanding, because it requires low electronic noise and high subtraction efficiencies over very large frequency bandwidths (from dc to a few times the repetition rate of the laser). Mostly as a result of these technical limitations, all the existing applications of the latter technique have been limited to pulse repetition rates well below the megahertz level.

Here we describe an efficient pulsed optical homodyne apparatus that operates in the time domain at the high repetition frequencies that are characteristic of commonly used mode-locked laser systems. We give a full characterization of our system by measuring the shot noise of a laser operating at a repetition rate of 82 MHz. We test the performances of the apparatus by comparing the results obtained by the time-domain technique with those from a more-conventional spectral approach; we also study the capability of the system to work in a gated configuration at lower acquisition rates, and we introduce an analysis based on the Allan variance to study the noise fluctuations on various time scales.

Finally, we present some results that exemplify the potential use of this technique for quantum state analysis by performing tomographic reconstructions of coherent states with low average photon numbers ($\langle n \rangle \sim 1$).

2. EXPERIMENTAL APPARATUS

A schematic of the experimental apparatus for homodyne measurements is shown in Fig. 1. A mode-locked Ti:sapphire laser (Spectra-Physics Tsunami), emitting trains of 3-ps pulses at 786 nm and at a repetition rate of 82 MHz, is used as a source for the local-oscillator (LO) beam. The total laser power can be varied by means of a half-wave plate followed by a polarizer. A 50% cube beam splitter mixes the LO with the field state under study, and two 80-mm lenses focus the output beams onto the photodetectors. Because the beam splitter is not perfectly insensitive to polarization, the balance between its two output ports is finely adjusted by use of half-wave plates. For measurement of the laser shot noise, the signal port

0740-3224/2002/051189-06$15.00

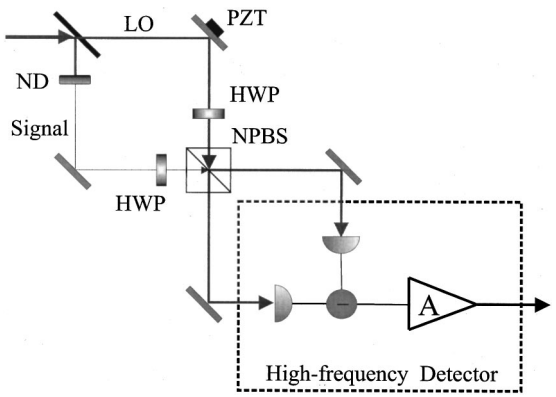

Fig. 1. Experimental setup: HWPs, half-wave plates; NPBS, nonpolarizing beam splitter; A, amplifier; PZT, piezoelectric translation stage; ND, neutral-density filter.

of the beam splitter is blocked, so only the vacuum field enters the apparatus.

Two p–i–n photodiodes (PDs; EG&G FFD040) are connected and oppositely biased. The signal generated on a load resistor is amplified with gain $G = 10$ by an operational amplifier (Comlinear CLC 425) in a noninverting configuration. The output signal is recorded by a spectrum analyzer or by a digital scope (LeCroy LC564) with a bandwidth of 1 GHz, a sampling rate of 4 Gsamples/s, a vertical resolution of 8 bits, and a storage depth of 200,000 points. We measured the overall detection efficiency η by comparing the reading of a powermeter with the mean photocurrent, obtaining a value of $\eta = 0.71 \pm 0.04$.

3. VACUUM FLUCTUATIONS: FREQUENCY ANALYSIS

We measured the frequency response of the single amplified PDs by illuminating them with the thermal light from a halogen lamp. A typical measured spectrum is shown in Fig. 2 for a photocurrent of 1.16 mA. By directing the laser pulse train onto the PDs we verified that their frequency-response curve is broad enough to isolate single pulses in the detected signal. The output pulses show a FWHM duration of ~5 ns, and successive pulses, separated by 12 ns, are clearly distinct from one another, as shown in the inset of Fig. 2. This is the first important property when we want to perform measurements only of particular events, selected by an external gate. The high temporal resolution minimizes the overlap of adjacent pulses. A fit of the output pulses with a double exponential function showed that 93% of the pulse energy is contained within the 12-ns window.

Another key property of the apparatus is its ability to efficiently subtract the amplitude fluctuations of the beams impinging upon the two detectors. This ability is expressed by the common mode rejection ratio (CMRR) of the balanced detection, defined as the spectral power measured when both PDs are illuminated, divided by the power measured on one PD when the other one is blocked. We measured it at the harmonic frequencies of the laser repetition rate, obtaining CMRRs of 42, 15, and 20 dB, respectively for the first, second, and third harmonics of the laser repetition rate. The higher harmonics exhibit lower CMRRs owing to the different responses of the PDs at higher frequencies.

We obtained the best CMRR by optimizing both the half-wave plate of the balanced detection and the bias of each PD. The measurements were performed at low laser power to prevent saturation of the amplifier by the unbalanced photocurrent when one PD was blocked.

We performed a more-stringent test on the effective capability of the detection system really to measure the quantum fluctuations of the signal in spite of the nonideal characteristics of the LO and of the detectors. We have indeed verified that, when the input signal was the vacuum state, we could measure the shot noise of the local oscillator. We obtained the measurement by acquiring the noise spectra for several values of the laser power impinging upon the PDs.

The frequency integral of the power spectrum is plotted in Fig. 3 as a function of the detected power, together with a second-order polynomial fit. We carried out the integration between 300 kHz and 150 MHz, excluding the

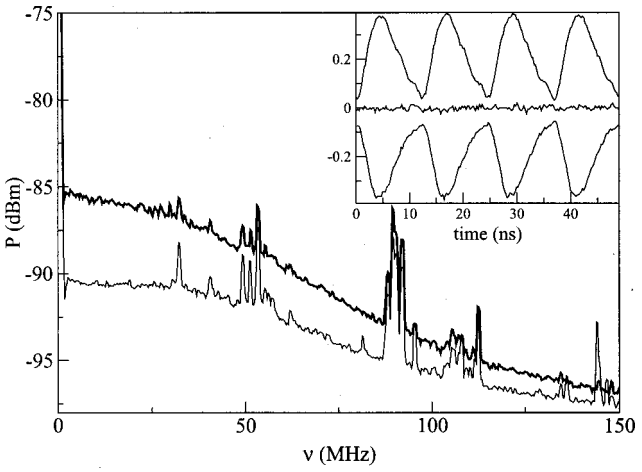

Fig. 2. Thicker curve, spectral power of the detected signal when one photodiode is illuminated by thermal light, giving a photocurrent of 1.16 mA. The resolution bandwidth is 300 kHz. Thinner curve, electronic noise. The narrow peaks are due to pickup from environmental noise. Inset, time-domain output signal with the laser impinging on only one photodiode (the upper and the lower traces correspond to the signals from the two detectors) and on both photodiodes (middle trace).

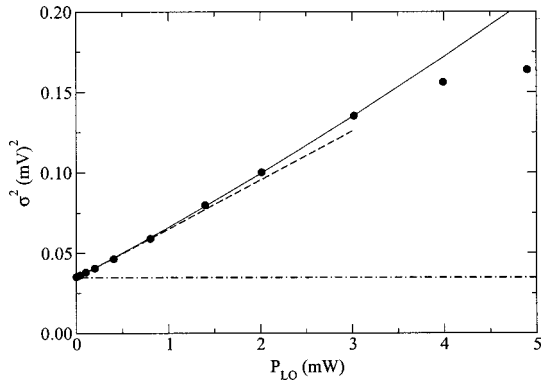

Fig. 3. Filled circles, integral of the power spectrum; solid curve, quadratic fit; dashed curve, shot-noise contribution; dashed–dotted curve, electronic noise.

peak at the laser repetition rate. The constant term of the fitting function gives the electronic and thermal noise; the first-order term corresponds to the laser shot noise (indicated in Fig. 3 by a dashed curve); the second-order term is due to the residual laser excess noise after the balanced detection. The relevant signal in homodyne detection is carried by the first-order term, whereas both the constant and the second-order terms give rise to unwanted excess Gaussian fluctuations. The optimum working power is ~3 mW; ~70% of the fluctuations can be attributed to the first-order term. Above this power, saturation effects appear. Saturation is frequency dependent: In the dc signal it does not appear until ~15 mW, whereas it becomes more important for the higher frequencies. To prevent signal distortion and doubtful measurements, we limited the laser power to 3 mW.

4. VACUUM FLUCTUATIONS: TIME-RESOLVED ANALYSIS

The spectral analysis described above applies particularly well to a quasi-cw measurement system. Indeed, the spectral properties are measured by the spectrum analyzer by means of time integration over the sequence of laser pulses. Instead, our apparatus has the important additional property that the detection bandwidth permits pulse-selective experiments to be performed. It is therefore possible to evaluate properties of the pulsed light by considering the different pulses as separate events.

In this section we report the experimental results obtained by means of three analyzing techniques used to characterize the pulsed time-resolved regime, namely, an off-line study of the variance of the pulse energy in time series, a more-refined investigation on different time scales based on the Allan variance, and, finally, the analysis of the fluctuations in laser pulses randomly acquired at a low rate.

For the off-line analysis, the output difference signal from the amplifier is stored in a digital scope. We numerically integrated time sequences of 200,000 samples, covering time windows of 50 μs and including 4000 pulses each, over time intervals of length $T = 12$ ns, corresponding to the separation between successive pulses, to extract the areas of all the pulses in the sequence and perform some statistics.

First we evaluated the variance σ_{PE}^2 of the pulse energy over the recorded time series for several values of the laser average power, as shown in Fig. 4. This time-resolved analysis is directly related to the spectral analysis by

$$\sigma_{\mathrm{PE}}^2 = 2\int_0^\infty S(\nu)F(\nu)d\nu, \tag{1}$$

where $F(\nu)$ is the weight function that is due to the time integration over the rectangular window that corresponds to pulse duration T; that is,

$$F(\nu) = T^2\frac{\sin^2(\pi\nu T)}{(\pi\nu T)^2}. \tag{2}$$

The variance σ_{PE}^2 evaluated from the measured noise spectra according to Eq. (1) is also shown in Fig. 4. Good agreement with the direct time-domain measurements is shown, thus confirming the correctness of our approach.

Afterward, we performed a more-refined time-resolved analysis of the pulse sequences stored in the scope. The study was based on the Allan variance σ_A^2, defined as[7]

$$\sigma_A^2(\tau) = 1/2\langle(f_{2,\tau} - f_{1,\tau})^2\rangle, \tag{3}$$

where $f_{1,\tau}$ and $f_{2,\tau}$ are the integrals of the time-dependent signal $f(t)$ over two adjacent time intervals, both of duration τ. The angle brackets indicate averaging over the whole time sequence.

The Allan variance is a widely used indicator in metrology and allows the stability of a parameter to be quantified on different time scales.

In a time-resolved analysis, σ_A^2 has a role similar to that of spectral density $S(\nu)$ in the spectral analysis. Spectral density $S(\nu)$ and the Allan variance are indeed related by the Cutler theorem

$$\sigma_A^2(\tau) = 4T^2\int_0^\infty S(\nu)\frac{\sin^4(\pi\nu\tau)}{(\pi\nu\tau)^2}d\nu. \tag{4}$$

In our case of discretized time intervals, σ_A^2 is significant only when it is calculated over integer multiples $\tau = nT$ of pulse separation T. In Fig. 5 we show a comparison of the Allan variance measured in the time domain and that obtained by integration of the noise spectral power by use of Eq. (4).

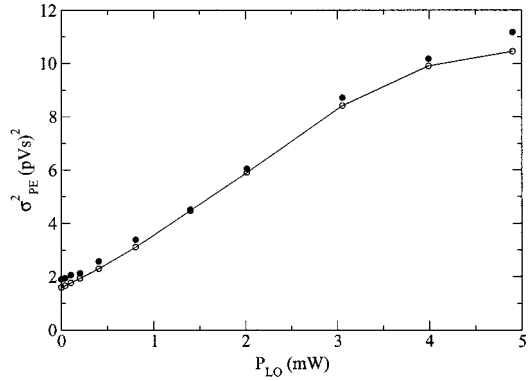

Fig. 4. Filled circles, directly measured σ_{PE}^2; open circles, variance deduced from the spectrum according to Eq. (1).

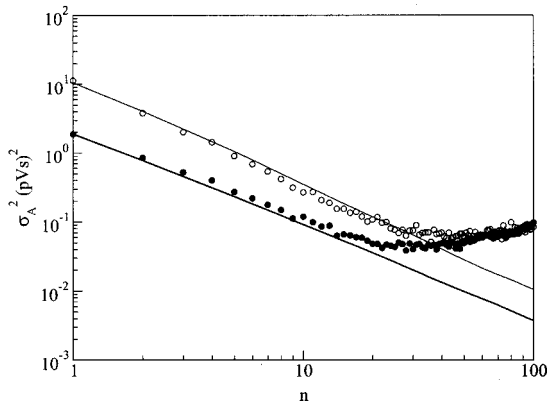

Fig. 5. Allan variance of the pulse energy. Open circles, laser power of 3 mW; filled circles, electronic noise; solid curves, Allan variances calculated from the spectrum according to Eq. (4). The abscissa is in units of pulse separation T.

Analysis of $\sigma_A^2(\tau)$ showed a τ^{-1} dependence for short τ that corresponds to a white-noise spectrum at high frequencies. As has already been discussed, this spectrum contains contributions from electronic noise, shot noise, and excess noise. For longer $\tau (\gtrsim 20T)$, we observed that the directly measured $\sigma_A^2(\tau)$ flattened as a result of $1/f$ noise. However, the variance deduced from the noise spectrum through Eq. (4) did not deviate from the linear behavior observed for short τ. This discrepancy is due to low-frequency fluctuations in the digital scope electronics. A better preamplifier should allow for accurate measurements at least up to $\tau = 100T$.

We can conclude that our apparatus can be efficiently used to detect quantum states in a homodyne experiment in which the pulsed laser supplies the local oscillator, at least for time scales up to ~ 1 μs. The most useful time scale can be chosen according to the specific experiment and to the kind of optical field to be analyzed. We remark that an appropriate choice of the time scale for σ_A^2 can provide an opportunity to observe and analyze quantum effects that are overwhelmed by classical fluctuations for longer time scales in a way similar to what happens in the frequency analysis when one chooses a particular spectral region.

A deeper analysis permits a better understanding of the properties of σ_A^2 and σ_{PE}^2. If we consider, in particular, $\sigma_A^2(T)$ by comparing Eqs. (1) and (2) with Eq. (4), we can see that the weight function that multiplies $S(\nu)$ in the integral decreases as $(\nu\tau)^2$ for small ν in Eq. (4), whereas it remains constant in the expressions for σ_{PE}^2. As a consequence, σ_{PE}^2 is more sensitive to excess low-frequency noise and indeed diverges in presence of $1/f$ noise. This divergence is eliminated by the cutoff imposed, for example, by the limited measurement time. However, the excess fluctuations are still present in the non-shot-noise terms of Fig. 4. They increase for longer measurement times and can eventually compromise the measurement possibilities.

The previous discussion has shown that, at least up to a time window of 50 μs, σ_{PE}^2 yields satisfactory results. It is now interesting to extend the analysis to discover whether our apparatus allows σ_{PE}^2 to be used for longer measurement times. Even if the excess low-frequency fluctuations prevent appreciation of quantum effects that occur on long time scales, we stress that σ_{PE}^2 contains information on the fluctuations that occur at all the time scales; therefore it remains a significant indicator as long as the contributions that arise from short-term quantum effects are not overwhelmed. A test at long time windows is particularly significant because some important experimental schemes require analyzing only interesting pulses, selected by independent measurement. In this case the acquisition of a single pulse must be triggered by an external gate and usually takes place at a much lower rate, so a long observation time is necessary to produce a statistically significant set of data.

As an example, one can consider the detection of Fock states obtained by parametric generation of twin beams in a $\chi^{(2)}$ medium and subsequent collapse of the signal wave function onto a number state, induced by photon counting on the idler channel. The use of a laser source similar to ours and typical nonlinear crystals will give an efficiency of $\beta \sim 10^{-2}$ for the generation of a single-photon state induced by each laser pulse. The probability of generation of an n-photon state scales as β^n, so, e.g., only one pulse of 10^6 will on average give rise to a three-photon state. Taking into account the 82-MHz repetition rate of the laser leads to $\sim 10^2$ counts/s if one wants to measure the properties of the three-photon Fock state.

We simulated this situation by triggering the scope synchronously with the laser repetition rate but acquiring single pulses instead of sequences. Each pulse area was measured directly by the scope, and the statistics were collected on line by the scope's internal data analysis software. The acquisition rate was reduced to ~ 50 pulses/s. With respect to the off-line analysis of 50-μs series, this setup was clearly more sensitive to possible low-frequency noise fluctuations; however, no increase in the measured variance of the pulse energy was observed for measurement times of at least 1 min. Based on this result, it appears realistic to tackle the problem of tomographic reconstruction, in a time of the order of minutes, of the three-photon Fock state considered above.

5. HOMODYNE TOMOGRAPHY

To perform a test of actual homodyne tomography with our high-frequency acquisition technique we slightly modified the experimental apparatus as shown in Fig. 1. A fraction of the laser power was split off the main (LO) beam and entered the second port of the beam splitter. We first achieved a good spatiotemporal overlap between this signal field and the LO by carefully adjusting the alignment mirrors and the path lengths by means of two optical delay lines (not shown in the figure) to obtain high-visibility interference fringes. Then the signal beam was strongly attenuated by means of calibrated neutral-density filters and the beam path length in the LO arm was correspondingly compensated for. We controlled the relative phase between the two fields by applying a voltage to a piezoelectric transducer holding one of the mirrors in the LO's beam path.

We performed measurements of coherent states with several average photon numbers that ranged from 0 to ~ 5. Each measurement consisted of 8 sequences of 4000 pulses for each of the 25 values of the relative phase in the $[0, \pi]$ interval, for a total of 800,000 points per coherent state.

For each value of relative phase θ between the LO field and the signal field, the histogram of the measured pulse energy difference represents the distribution $P_\theta(x)$ of the specific phase-rotated quadrature x. Collection of the distributions $P_\theta(x)$ for all θ permits the tomographic reconstruction of the quantum state of the radiation field. The tomographic reconstruction methods permit Wigner function $W(x, y)$ to be obtained in quadrature phase-space[5] or density matrix elements ρ_{nm} to be expressed on a Fock basis.[8]

The reconstruction of the Wigner function is based on the fact that the distributions $P_\theta(x)$ are the marginal integrals of the Wigner function[9]

$$P_\theta(x) = \int_{-\infty}^{+\infty} W(x\cos\theta - y\sin\theta,\ x\sin\theta + y\cos\theta)dy. \tag{5}$$

Because the set of marginal distributions $\{P_\theta(x):\theta \in [0, \pi]\}$ represents the Radon transform of the Wigner function, we can obtain the Wigner function by applying the inverse transformation to the measured $P_\theta(x)$. However, this method introduces an arbitrary cutoff parameter, which should be carefully chosen to avoid the introduction of artifacts into the reconstructed function. In Fig. 6 we show the reconstructed Wigner functions for the vacuum state (detected when the signal beam is blocked at the input of the homodyne beam splitter) and for a weak coherent field with a mean photon number $\langle n\rangle \sim 1$.

The second reconstruction procedure, called the quantum sampling method, permits the density matrix elements to be reconstructed without the introduction of any arbitrary parameter and also directly gives an estimation of the reconstruction errors. Probability distributions $P_\theta(x)$ are transformed according to

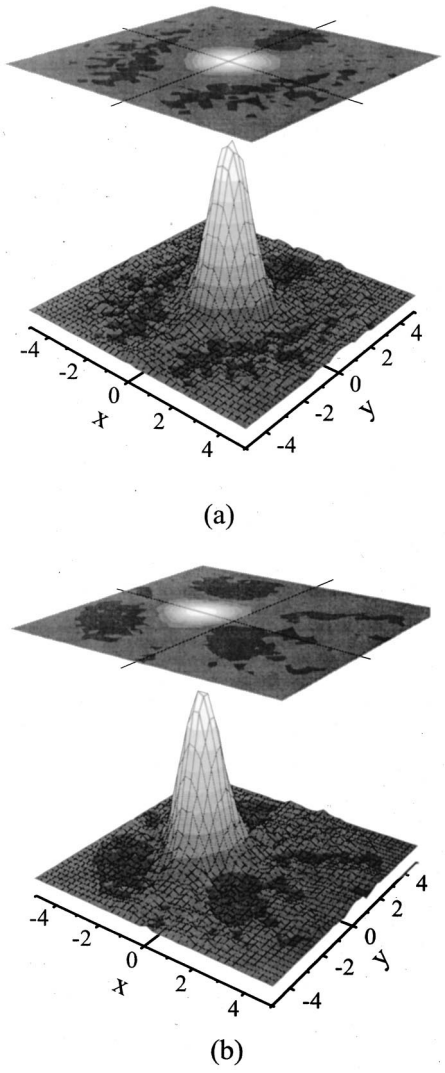

Fig. 6. Reconstructed Wigner functions: (a) vacuum state, (b) weak coherent state with $\langle n\rangle \sim 1$.

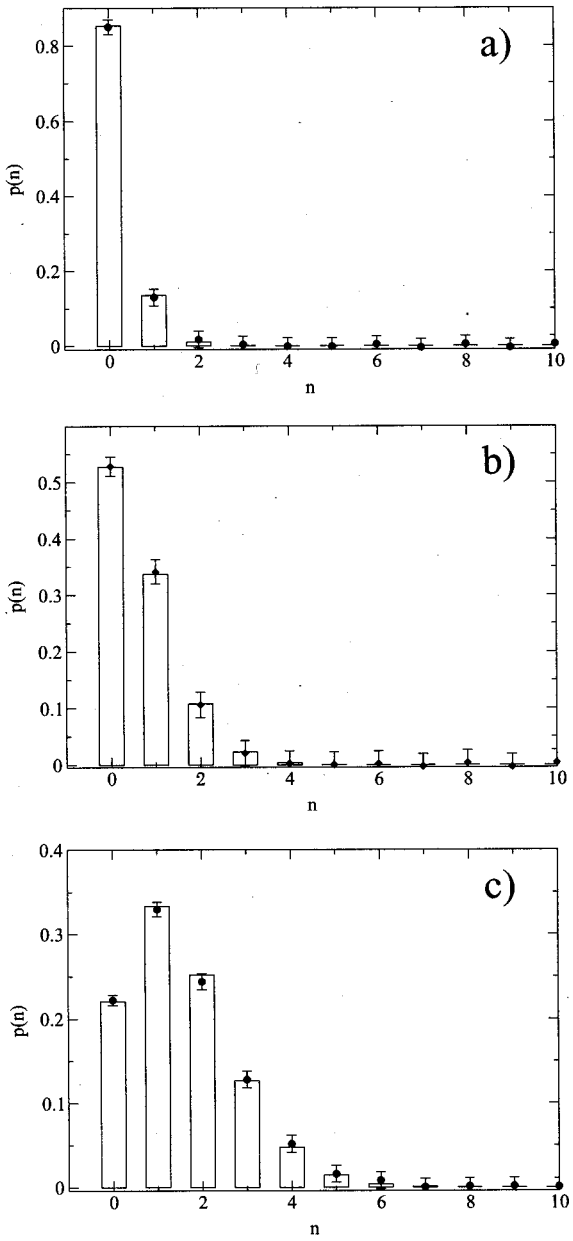

Fig. 7. Reconstruction of the photon statistics of three coherent states. The filled circles with error bars are the reconstructed values. Rectangles, best-fit Poissonian distribution values with (a) $\langle n\rangle = 0.16$ photons/pulse, (b) $\langle n\rangle = 0.64$ photons/pulse, and (c) $\langle n\rangle = 1.5$ photons/pulse.

$$\rho_{nm} = \langle n|\hat{\rho}|m\rangle = \frac{1}{\pi}\int_0^\pi d\theta \int_{-\infty}^{+\infty} dx P_\theta(x) f_{nm}(x)[\exp i(n-m)\theta], \tag{6}$$

where f_{nm} are the factorized kernel functions, called sampling functions.[10] The reconstructed diagonal elements of density matrix ρ_{nm} are shown in Fig. 7 for three coherent states with different mean photon numbers. These values are well fitted by Poissonian distributions, as expected for coherent states.

6. CONCLUSIONS

We have described a detection system that is suitable for homodyne measurements of quantum states generated by pulsed radiation at a high repetition frequency. We have investigated the main features of a time-resolved analysis of the homodyne signal, characterizing the system response by means both of standard indicators and of the Allan variance. This investigation allows the most useful time scales to be chosen for better selection of the quantum properties of the field. The results compare well with those of a standard spectral analysis.

We have shown that our apparatus permits pulse-selective measurements at high repetition rates. This property is particularly useful for the study of rare events that are selected by an external gate. The use of high repetition rates has been proposed[11] as a way to circumvent the limitations in the generation and detection of quantum states connected with the finite efficiency of detectors. In a conditional homodyne measurement one has to be sure that n clicks in the detectors really correspond to n photons arriving at the measurement apparatus. This can be ensured only if the gain in the generation is kept sufficiently low as to have a negligible probability of generating $n + 1$ photons. Unfortunately, low gains also mean low production rates and impractically long acquisition times, unless much higher pump rates are used.

With respect to the current setups, which operate well below the megahertz level, our approach permits an improvement of at least 2 orders of magnitude in the acquisition rate. This results in two fundamental advantages: on one side, the stability requirements of the overall experimental system are relaxed; on the other, if long-term stability of the setup is available it is possible to reconstruct states with higher photon numbers that are generated at very low rates.

The demonstration of reliable quantum tomographic reconstruction at high frequencies opens new possibilities in the investigation of highly nonclassical states such as mesoscopic Fock[12] states generated by a low-efficiency parametric generator and quantum superpositions of macroscopic states (Schrödinger's catlike states), of the electromagnetic field.

ACKNOWLEDGMENTS

The authors acknowledge support from research project PRA-CAT 97 of the Istituto Nazionale di Fisica per la Materia (INFM).

A. Zavatta's e-mail address is azavatta@ino.it.

REFERENCE AND NOTES

1. S. Reynaud, A. Heidmann, E. Giacobono, and C. Fabre, "Quantum fluctuations in optical systems," in *Progress in Optics*, E. Wolf, ed. (Elsevier, Amsterdam, 1992), Vol. **30**, pp. 1–85.
2. U. Leonhardt, *Measuring the Quantum State of Light* (Cambridge U. Press, Cambridge, 1997).
3. G. Breitenbach, S. Schiller, and J. Mlynek, "Measurement of the quantum states of squeezed light," Nature **387**, 471–475 (1997).
4. M. Vasilyev, S.-K. Choi, P. Kumar, and G. M. D'Ariano, "Investigation of the photon statistics of parametric fluorescence in a traveling-wave parametric amplifier by means of self-homodyne tomography," Opt. Lett. **23**, 1393–1395 (1998).
5. D. Smithey, M. Beck, M. G. Raymer, and A. Faridani, "Measurement of the Wigner function distribution and the density matrix of a light mode using optical homodyne tomography: application to squeezed states and the vacuum," Phys. Rev. Lett. **70**, 1244–1247 (1993).
6. M. Crispino, G. Di Giuseppe, F. De Martini, P. Mataloni, and H. Kanatsoulis, "Towards a Fock-states tomographic reconstruction," Fortschr. Phys. **48**, 589–598 (2000).
7. D. W. Allan, "Statistics of atomic frequency standard," Proc. IEEE **54**, 221–230 (1966).
8. G. M. D'Ariano, C. Macchiavello, and M. G. A. Paris, "Detection of the density matrix through optical homodyne tomography without filtered back projection," Phys. Rev. A **50**, 4298–4302 (1994).
9. K. Vogel and H. Risken, "Determination of quasiprobability distribution in terms of probability distributions for rotated quadrature phase," Phys. Rev. A **40**, 2847–2849 (1989).
10. U. Leonhardt, M. Munroe, T. Kiss, Th. Richter, and M. G. Raymer, "Sampling of photon statistics and density matrix using homodyne detection," Opt. Commun. **127**, 144–160 (1996).
11. A. Montina and F. T. Arecchi, "Toward an optical evidence of quantum interference between macroscopically different states," Phys. Rev. A **58**, 3472–3476 (1998).
12. After the submission of this manuscript, A. I. Lvovsky, H. Hansen, T. Aichele, O. Benson, J. Mlynek, and S. Schiller, reported the quantum reconstruction of a single photon Fock state, using a laser repetition rate of 800 kHz, in "Quantum state reconstruction of the single-photon Fock state," Phys. Rev. Lett. **87**, 050402-1–4 (2001).